Infectious Disease Modelling 9 (2024) 975–994

Contents lists available at ScienceDirect

Infectious Disease Modelling

journal homepage: www.keaipublishing.com/idm

Parameter identifiability of a within-host SARS-CoV-2 epidemic model

Junyuan Yang [a, b, *], Sijin Wu [b], Xuezhi Li [c, **], Xiaoyan Wang [d], Xue-Song Zhang [e], Lu Hou [e]

[a] Complex Systems Research Center, Shanxi University, Taiyuan, 030006, China
[b] Shanxi Key Laboratory of Mathematical Techniques and Big Data Analysis on Disease Control and Prevention, Shanxi University, Taiyuan, 030006, China
[c] School of Mathematics and Science, Henan Normal University, Xinxiang, 453000, China
[d] School of Information, Shanxi University of Finance and Economics, Taiyuan, 030006, China
[e] Agriculture and Animal Husbandry Technology Promotion Center of Xingan League, Xingan League, 137400, China

ARTICLE INFO

Article history:
Received 5 March 2024
Received in revised form 9 May 2024
Accepted 10 May 2024
Handling Editor: Dr Daihai He

Keywords:
Structural identifiability
Practical identifiability
Sensitivity analysis
The basic reproduction number

ABSTRACT

Parameter identification involves the estimation of undisclosed parameters within a system based on observed data and mathematical models. In this investigation, we employ DAISY to meticulously examine the structural identifiability of parameters of a within-host SARS-CoV-2 epidemic model, taking into account an array of observable datasets. Furthermore, Monte Carlo simulations are performed to offer a comprehensive practical analysis of model parameters. Lastly, sensitivity analysis is employed to ascertain that decreasing the replication rate of the SARS-CoV-2 virus and curbing the infectious period are the most efficacious measures in alleviating the dissemination of COVID-19 amongst hosts.

1. Introduction

The term Corona Virus Disease 2019 (COVID-19) pertains to a form of pneumonia resulting from the invasion of the novel coronavirus in year 2019. It manifests as an exceptionally virulent and lethal ailment triggered by the severe acute respiratory syndrome coronavirus 2 (SARS-CoV-2). So far, approximately 7 million people worldwide have succumbed to this disease and 770 million cases being reported (World Health Organization). The sudden outbreak of COVID-19 has enormous pressure on the global economy and public health security. Since it is unethical to do experiments directly in the human body for evaluating the severity of an infection, mathematical modeling has emerged as a widely utilized approach to study the transmission dynamics of diseases aimed at mitigating the severe consequences of pandemic.

Indeed, there are numerous within-host and between-host models for studying the transmission behaviors of COVID-19 infection. The COVID-19 infection exhibits an incubation period of 5.2 days (95% confidence interval CI: 4.1 − 7.0), a discrete

* Corresponding author. Complex Systems Research Center, Shanxi University, Taiyuan, 030006, China.
** Corresponding author.
E-mail addresses: yjyang66@sxu.edu.cn (J. Yang), xzli66@126.com (X. Li).
Peer review under responsibility of KeAi Communications Co., Ltd.

https://doi.org/10.1016/j.idm.2024.05.004

span brimming with potentiality and anticipation. (Li et al., 2020a). Numerous scholars have used the framework of SEIR compartment to estimate the severity of the COVID-19 transmission (Tang et al., 2020; Teslya et al., 2020; Wu et al., 2020). Since then, asymptotic infection and severe infection are incorporated into mathematical modelling for evaluating the medical care requirement (Mizumoto et al., 2020; Moghadas et al., 2020; Odagaki, 2023). Furthermore, with the evolution of the COVID-19 infection, lots of non-pharmacological and pharmacological prevention measures had been taken for the mitigation of the disease spread (Bhavana et al., 2020; Marechal et al., 2020). For instance, non-pharmacological control strategies including household quarantine (Outbreak of acute respiratory syndrome, 2020), wearing face masks (Anderson et al., 2020; Guidelines for the use of, 2020) and clearing with an alcohol-based disinfectant (Kampf, 2018) had been used to extensively reduce the risk of the infection during its seasons. Additionally, mandatory curtailment of social gatherings (Sims et al., 2022; Wilder-Smith and Freedman, 2020) and the implementation of large-scale detection (Esbin et al., 2020) have been administered for government to curb COVID-19 spread.

In (Li et al., 2020b), Li et al. introduced a within-host model to elucidate the intricate dynamics among the healthy cells, infected cells, and SARS-CoV-2 within the human physique. Their seminal investigation revealed that prompt administration of suitable therapeutics can significantly diminish the pool of infected cells and expeditiously hasten the demise of SARS-CoV-2. Elbaz et al. added a latent stage into the model proposed by Li et al. (Li et al., 2020b), offering a new viewpoint on disease dynamics and a more realistic representation of disease progression (Elbaz et al., 2023). Moreover, numerous clinical studies have revealed the presence of the antibody-dependent enhancement phenomenon in the transmission of SARS-CoV-2 (Cloutier et al., 2020; Okuya et al., 2022; Sá et al., 2021). It is not hard to see that the existing results focus on the prediction of COVID-19 infection or the theoretical dynamics of the within-host models. In particular, Li et al. used the following ordinary differential equations (ODEs) to describe the kinetics of COVID-19 within host

$$\begin{cases} \dfrac{dE_p(t)}{dt} = d_E\big(E_p(0) - E_p(t)\big) - \beta E_p(t)v(t), \\ \dfrac{dE_p^*(t)}{dt} = \beta E_p(t)v(t) - d_{E^*}E_p^*(t), \\ \dfrac{dv(t)}{dt} = \pi_v E_p^*(t) - d_v v(t). \end{cases} \tag{1}$$

where $E_p(t)$ denotes the number of uninfected epithelial cells, $E_p^*(t)$ represents the quantity of infected epithelial cells and $v(t)$ is the amount of viruses. $E_p(0)$ is the value of uninfected epithelial cells when symptom onset. $d_E E_p(0)$ is the continuous reproduction of uninfected epithelial cells. The parameter β is the infection rate, π_v is the release rate of viral particles from deadly infected epithelial cells. Parameters d_E, d_{E^*}, d_v are the death rates of uninfected epithelial cells, infected epithelial cells and the viruses, respectively. In (Nath et al., 2021), Nath carried out the qualitative analysis of the within-host model (1). They defined the basic reproduction number of the model (1) by

$$R_0 = \frac{\pi_v \beta E_p(0)}{d_{E^*} d_v}. \tag{2}$$

The elucidation of the reproductive number, denoted as R_0, encapsulates the quantity of infected cells engendered by a singly infected cell within an entirely unblemished milieu throughout its lifespan. According to Lemmas 1–2, and Theorems 1–4 in (Nath et al., 2021), we get the following lemma on the stability of each feasible equilibrium.

Lemma 1.1. *Let R_0 be defined in (2). Then the following issues hold*:

(1) *If $R_0 < 1$, then the virus-free equilibrium $X^0 = (E_p(0), 0, 0)$ is globally asymptotically stable*;
(2) *When $R_0 > 1$, then the viral spread equilibrium $X^+ = (\overline{E_p}, \overline{E_p^*}, \overline{v})$ is globally asymptotically stable, where*

$$\overline{E_p} = \frac{d_{E^*} d_v}{\beta \pi_v} = \frac{E_p(0)}{R_0},\ \overline{E_p^*} = \frac{d_E d_v}{\beta \pi_v}(R_0 - 1),\ \overline{v} = \frac{d_E}{\beta}(R_0 - 1).$$

Parameter identification is the process of determining unknown parameters in a system through observed data and mathematical models.It is an important task in the field of system identification and is used to reveal the intrinsic characteristics and behavior of a system, while complex features and behaviors of a system often involve a large number of unknown parameters and epidemiological state variables. These variability and uncertainty always cause lack of accuracy in the predictions made by those mathematical models. Parameter identification is an important prerequisite to identify such concerned issues from theoretical and practical perspectives. In particular, the mathematical models with unidentifiable parameters could be multiple outcomes of the prediction and they may lead to inaccuracy prediction and made unsuitable control measures. Conversely, a model with identifiable parameters signifies a high degree of accuracy results from the

observations. Numerous papers have centered on the theoretical and numerical approaches of parameter identifiability. In (Miao et al., 2011), Miao et al. undertook a comprehensive examination of diverse methodologies pertaining to the assessment of both the structural and practical identifiability of models expounded through ordinary differential equations (ODEs). Miao et al. provide a concise overview of the various approaches to parameter identification. This paper extensively examines the structure and practical implementation of parameter identification by employing two methods within a within-host model. In (Tuncer et al., 2022), Tuncer et al. utilized a between-host COVID-19 model to examine parameter identifiability with the observed data of COVID-19 daily cases and deaths in the US. In (Tuncer et al., 2018), Tuncer et al. developed structurally identifiable analysis of Zika models, which showed that direct transmission rate was practically unidentifiable. We have noted that the mentioned articles above primarily investigate the parameter identifiability of macroscopic models. However, the scholars in Li (Li et al., 2020b) and Nath (Nath et al., 2021) solely undertook theoretical examination pertaining to the model and prognostication of the ailment, inadvertently neglecting the crucial aspect of parameter identifiability within the aforementioned proposed framework. To fill this gap, we employ the model proposed in (Li et al., 2020b) to investigate the parameter identifiability, encompassing both its structural aspects (assuming noiseless data) and its practical implications (using real data).

The main contributions of this paper consists of two aspects: To our knowledge, we first investigate structurally and practically identifiable analysis for a microcosmic model of SARS-CoV-2 infection. We find that the parameters are globally identifiable when all state variables are observed, but they are unidentifiable if the infected cells or the virus load are measured. However, the findings of the sensitivity analysis indicate that focusing on curbing the propagation of SARS-CoV-2 within hosts can be most efficacious when targeting both the infection rate and the mortality rate of infected cells.

The reminder of this paper is organized as follows: In Section 2, we explore several types of structural identifiability of model parameters, such as scenarios when alternative data for state variables are available. We further conduct practical identifiability analysis by using the infected cells data from Li et al. (Li et al., 2020b) and the virus load from Zheng et al. (Zheng et al., 2020) in Section 3. We conduct Monte Carlo simulations on a constrained minimization conundrum and quantify the average relative estimation errors of parameters amidst Gaussian and Poisson noise levels, aiming to investigate its practical identifiability. In Section 4, we delve into the intricacies of sensitivity analysis applied to the within-host model, assessing the profound depths of influence that variations in paramount parameters wield upon the intensity of an infectious ailment. In the last section, we summarize our findings and draw some interesting conclusions.

2. Structural identifiability analysis of the immunological SARS-CoV-2 model

Structural identifiability concerns the retrieval of model parameters based on the observed outputs. In this section, we undertake an analysis of the structural identifiability to ascertain the uniqueness of values of the parameters for model (1) using the available observations. In other words, the model parameters are said to be globally structural identification for the given ideal conditions of noise-free observations and error-free model structure. For given large enough data sets, there are infinite sets of parameter values that can produce the same observations, then the model parameters are said to be non-identifiable. If there exist finite (greater than one) sets of parameters that result in identical observations, then the parameters of the model are deemed to possess local identifiability.

Without loss of generality, we write model (1) as below:

$$\begin{aligned} &x^{'}(t) = f(x(t), p), \quad x(0) = x_0, \\ &y(t) = g(x(t), p), \end{aligned}$$

where $x = \{E_p, E_p^*, v\} \in \mathbb{R}^3$ denote the states variables, $x(0)$ are the initial values of state variables. y represent output vectors, such as the infected pulmonary epithelial cells, and p denotes the parameters of system (1). We first introduce some related definitions of structurally identifiable analysis given in (Miao et al., 2011).

Definition 2.1. A parameter set p are called globally (or uniquely) structurally identifiable if for every q in the parameter space

$$g(x(t), p) = g(x(t), q) \Longleftrightarrow p = q.$$

Definition 2.1 suggests that a slight difference in parameter values will result in distinct model predictions or outputs when one uses the noise-free data. In other words, if $p \neq q$, then $g(x(t), p) \neq g(x(t), q)$ (i.e. If every observation of the mathematical model can solely be ascertained through an exceptional combination of parameters, then it is referred to as structurally globally or uniquely identifiable).

Definition 2.2. The parameter set p display local identifiability if there exists a neighborhood $\mathbb{N}(p)$ surrounding p such that if g(x(t), p) = g(x(t), q) for $q \in \mathbb{N}(p)$ then $p = q$.

As we know, the differential algebra approach (Bellu et al., 2007) is an useful tool to check the structural identifiability of the parameters in model (1). One of the merits inherent in this particular approach lies in its capacity to acquire not only non-identifiable parameters but also the conceivable permutations thereof, in the event that the result is deemed unidentifiable. Subsequently, these parameters can be employed to reparameterize the initial model in a manner that engenders a structural identifiability of all parameters. This approach unveils the input-output equation encompassing the entirety of structurally identifiable information pertaining to the parameters. This equation is a valuable tool for analyzing and understanding the identifiable properties of the model. Now, we obtain the input-output equations of the model (1) using the observation values of chest radiograph score that reflecting the severity of infected pulmonary epithelial cells $E_p^*(t)$, that is $y_1(t) = E_p^*(t)$ along with known initial conditions, $E_p(0) = 25$, $E_p^*(0) = 2.59$, $v(0) = 0.061$. The data from articles (Li et al., 2020b) and (Zheng et al., 2020).

Theorem 2.3. *The epidemiological model (1) is not structural identifiability of the parameters β and π_v from the known infected cells $E_p^*(t)$. But the parameters $d_E, E_p(0), d_{E^*}, d_v$, and the combinations of $\beta\pi_v$ can be identified.*

Proof. Using DAISY (Bellu et al.), we eliminate the unknown state variables $E_p(t)$ and $v(t)$ to obtain the following input-output equation:

$$
\begin{aligned}
0 = {} & \left(\frac{d^3y_1}{dt^3}\right)^2\frac{dy_1}{dt}y_1 + d_{E^*}\left(\frac{d^3y_1}{dt^3}\right)^2 y_1^2 - a_1\left(\frac{d^3y_1}{dt^3}\right)^2 y_1 - \frac{d^3y_1}{dt^3}\left(\frac{d^2y_1}{dt^2}\right)^2 y_1 - \frac{d^3y_1}{dt^3}\frac{d^2y_1}{dt^2}\left(\frac{dy_1}{dt}\right)^2 \\
& + a_2\frac{d^3y_1}{dt^3}\frac{d^2y_1}{dt^2}\frac{dy_1}{dt}y_1 + a_1\frac{d^3y_1}{dt^3}\frac{d^2y_1}{dt^2}\frac{dy_1}{dt} + 2a_3\frac{d^3y_1}{dt^3}\frac{d^2y_1}{dt^2}y_1^2 + a_4\frac{d^3y_1}{dt^3}\frac{d^2y_1}{dt^2}y_1 \\
& - a_5\frac{d^3y_1}{dt^3}\left(\frac{dy_1}{dt}\right)^3 + 4a_6\frac{d^3y_1}{dt^3}\left(\frac{dy_1}{dt}\right)^2 y_1^2 + a_8\frac{d^3y_1}{dt^3}\left(\frac{dy_1}{dt}\right)^2 y_1 + a_1a_5\frac{d^3y_1}{dt^3}\left(\frac{dy_1}{dt}\right)^2 \\
& + 8a_7\frac{d^3y_1}{dt^3}\frac{dy_1}{dt}y_1^3 + a_9\frac{d^3y_1}{dt^3}\frac{dy_1}{dt}y_1^2 + a_1a_{10}\frac{d^3y_1}{dt^3}\frac{dy_1}{dt}y_1 + 4d_{E^*}a_7\frac{d^3y_1}{dt^3}y_1^4 + a_{11}\frac{d^3y_1}{dt^3}y_1^3 \\
& + a_{12}\frac{d^3y_1}{dt^3}y_1^2 + \left(\frac{d^2y_1}{dt^2}\right)^3\frac{dy_1}{dt} + b_1\left(\frac{d^2y_1}{dt^2}\right)^3 y_1 + b_2\left(\frac{d^2y_1}{dt^2}\right)^2\left(\frac{dy_1}{dt}\right)^2 - 3a_6\left(\frac{d^2y_1}{dt^2}\right)^2\frac{dy_1}{dt}y_1^2 \\
& + b_4\left(\frac{d^2y_1}{dt^2}\right)^2\frac{dy_1}{dt}y_1 + a_1b_3\left(\frac{d^2y_1}{dt^2}\right)^2\frac{dy_1}{dt} - 3a_7\left(\frac{d^2y_1}{dt^2}\right)^2 y_1^3 + b_5\left(\frac{d^2y_1}{dt^2}\right)^2 y_1^2 \\
& + a_1b_6\left(\frac{d^2y_1}{dt^2}\right)^2 y_1 + b_7\frac{d^2y_1}{dt^2}\left(\frac{dy_1}{dt}\right)^3 + 2a_6b_8\frac{d^2y_1}{dt^2}\left(\frac{dy_1}{dt}\right)^2 y_1^2 + b_9\frac{d^2y_1}{dt^2}\left(\frac{dy_1}{dt}\right)^2 y_1 \\
& + a_1b_{10}\frac{d^2y_1}{dt^2}\left(\frac{dy_1}{dt}\right)^2 + 2a_7b_{11}\left(\frac{d^2y_1}{dt^2}\right)^2\frac{dy_1}{dt}y_1^3 + b_{12}\frac{d^2y_1}{dt^2}\frac{dy_1}{dt}y_1^2 + a_1b_{13}\frac{d^2y_1}{dt^2}\frac{dy_1}{dt}y_1 \\
& + 2a_7d_{E^*}(b_2 + 3d_v)\frac{d^2y_1}{dt^2}y_1^4 + d_{E^*}b_{14}\frac{d^2y_1}{dt^2}y_1^3 + a_1b_{15}\frac{d^2y_1}{dt^2}y_1^2 - a_6\left(\frac{dy_1}{dt}\right)^5 + a_6c_1\left(\frac{dy_1}{dt}\right)^4 y_1 \\
& + c_3\left(\frac{dy_1}{dt}\right)^4 + 4a_6^2\left(\frac{dy_1}{dt}\right)^3 y_1^3 + a_6c_2\left(\frac{dy_1}{dt}\right)^3 y_1^2 + c_4\left(\frac{dy_1}{dt}\right)^3 y_1 + a_1c_5\left(\frac{dy_1}{dt}\right)^3 \\
& + 12d_{E^*}a_6^2\left(\frac{dy_1}{dt}\right)^2 y_1^4 + a_6c_6\left(\frac{dy_1}{dt}\right)^2 y_1^3 + c_7\left(\frac{dy_1}{dt}\right)^2 y_1^2 + a_1c_8\left(\frac{dy_1}{dt}\right)^2 y_1 + 12a_7^2\frac{dy_1}{dt}y_1^5 \\
& + a_7c_9\frac{dy_1}{dt}y_1^4 + c_{10}\frac{dy_1}{dt}y_1^3 + c_{11}\frac{dy_1}{dt}y_1^2 + 4d_1y_1^6 + d_2y_1^5 + d_3y_1^4 + d_4y_1^3,
\end{aligned}
\tag{3}
$$

where

$$a_1 = d_E E_p(0), \quad a_2 = 2d_E - d_{E^*} + 2d_\nu, \quad a_3 = d_{E^*}(d_E + d_{E^*} + d_\nu),$$
$$a_4 = -d_E E_p(0)(3d_E + 2d_{E^*} - 3d_\nu), \quad a_5 = d_E + d_{E^*} + d_\nu, \quad a_6 = \beta\pi_\nu,$$
$$a_7 = \beta d_{E^*}\pi_\nu, \quad a_8 = d_E^2 + 2d_E d_\nu - 2d_{E^*}^2 + d_\nu^2,$$
$$a_9 = -8\beta d_E E_p(0)\pi_\nu + 2d_E^2 d_{E^*} + d_E d_{E^*}^2 + 4d_E d_{E^*} d_\nu + d_{E^*}^2 d_\nu + 2d_{E^*} d_\nu^2,$$
$$a_{10} = -d_E^2 - 2d_E d_{E^*} - 2d_E d_\nu - 2d_{E^*} d_\nu - d_\nu^2,$$
$$a_{11} = d_{E^*}\Big(-8\beta d_E E_p(0)\pi_\nu + d_E^2 d_{E^*} + 2d_E d_{E^*} d_\nu + d_{E^*} d_\nu^2\Big),$$
$$a_{12} = d_E E_p(0)\Big(4\beta d_E E_p(0)\pi_\nu - d_E^2 d_{E^*} - 2d_E d_{E^*} d_\nu - d_{E^*} d_\nu^2\Big),$$
$$b_1 = -2d_E - d_{E^*} - d_\nu, \quad b_2 = d_E + 2d_{E^*}, \quad b_3 = d_E + d_{E^*} + 2d_\nu,$$
$$b_4 = -d_E^2 - 3d_E d_{E^*} + d_E d_\nu - 2d_{E^*}^2 - d_{E^*} d_\nu + d_\nu^2,$$
$$b_5 = 2\beta d_E E_p(0)\pi_\nu - d_E^2 d_{E^*} + 2d_E d_{E^*}^2 + d_E d_{E^*} d_\nu + d_{E^*}^3 + 2d_{E^*}^2 d_\nu + d_{E^*} d_\nu^2,$$
$$b_6 = -2d_E^2 - 3d_E d_{E^*} - 5d_E d_\nu - d_{E^*}^2 - 3d_{E^*} d_\nu - 2d_\nu^2,$$
$$b_7 = d_E d_{E^*} - 2d_E d_\nu + 2d_{E^*}^2 - d_{E^*} d_\nu - 2d_\nu^2, \quad b_8 = d_E - d_{E^*} + 3d_\nu,$$
$$b_9 = 2\beta d_E E_p(0)\pi_\nu - d_E^2 d_{E^*} + 3d_E^2 d_\nu - 4d_E d_{E^*}^2 + 4d_E d_\nu^2 - 2d_{E^*}^3 - 3d_{E^*}^2 d_\nu - d_{E^*} d_\nu^2 + d_\nu^3,$$
$$b_{10} = d_E^2 + 3d_E d_{E^*} + 4d_E d_\nu + d_{E^*}^2 + 5d_{E^*} d_\nu + 3d_\nu^2,$$
$$b_{11} = 2d_E + d_{E^*} + 6d_\nu,$$
$$b_{12} = -8\beta d_E^2 E_p(0)\pi_\nu - 2\beta d_E d_{E^*} E_p(0)\pi_\nu - 12\beta d_E E_p(0) d_\nu\pi_\nu + 6d_E^2 d_{E^*} d_\nu + d_E d_{E^*}^3 + 4d_E d_{E^*}^2 d_\nu$$
$$+8d_E d_{E^*} d_\nu^2 + d_{E^*}^3 d_\nu + 2d_{E^*}^2 d_\nu^2 + 2d_{E^*} d_\nu^3,$$
$$b_{13} = -2\beta d_E E_p(0)\pi_\nu - d_E^3 - 4d_E^2 d_{E^*} - 5d_E^2 d_\nu - 2d_E d_{E^*}^2 - 8d_E d_{E^*} d_\nu$$
$$-5d_E d_\nu^2 - 2d_{E^*}^2 d_\nu - 2d_{E^*} d_\nu^2 - d_\nu^3,$$
$$b_{14} = -8\beta d_E^2 E_p(0)\pi_\nu - 8\beta d_E d_{E^*} E_p(0)\pi_\nu - 12\beta d_E E_p(0) d_\nu\pi_\nu + d_E^2 d_{E^*}^2 + 3d_E^2 d_{E^*} d_\nu$$
$$+2d_E d_{E^*}^2 d_\nu + 4d_E d_{E^*} d_\nu^2 + d_{E^*}^2 d_\nu^2 + d_{E^*} d_\nu^3,$$
$$b_{15} = 6\beta d_E^2 E_p(0)\pi_\nu + 4\beta d_E d_{E^*} E_p(0)\pi_\nu + 6\beta d_E E_p(0) d_\nu\pi_\nu - d_E^3 d_{E^*} - d_E^2 d_{E^*}^2$$
$$-5d_E^2 d_{E^*} d_\nu - 2d_E d_{E^*}^2 d_\nu - 5d_E d_{E^*} d_\nu^2 - d_{E^*}^2 d_\nu^2 - d_{E^*} d_\nu^3,$$
$$c_1 = -3d_{E^*} - 4d_\nu, \quad c_2 = d_E^2 + 2d_E d_{E^*} + 6d_E d_\nu - 6d_{E^*}^2 - 6d_{E^*} d_\nu + d_\nu^2,$$
$$c_3 = 2\beta d_E E_p(0)\pi_\nu - d_E^2 d_\nu + d_E d_{E^*}^2 - 2d_E d_{E^*} d_\nu - 2d_E d_\nu^2 + d_{E^*}^3 - 2d_{E^*} d_\nu^2 - d_\nu^3,$$
$$c_4 = 6\beta d_E d_{E^*} E_p(0)\pi_\nu + 8\beta d_E E_p(0) d_\nu\pi_\nu + d_E^3 d_\nu - d_E^2 d_{E^*}^2 + 2d_E^2 d_\nu^2 - d_E d_{E^*}^3 - 3d_E d_{E^*}^2 d_\nu$$
$$-2d_E d_{E^*} d_\nu^2 + d_E d_\nu^3 - d_{E^*}^3 d_\nu - 3d_{E^*}^2 d_\nu^2 - 2d_{E^*} d_\nu^3,$$
$$c_5 = -\beta d_E E_p(0)\pi_\nu + d_E^2 d_{E^*} + d_E^2 d_\nu + d_E d_{E^*}^2 + 4d_E d_{E^*} d_\nu + 2d_E d_\nu^2 + 2d_{E^*}^2 d_\nu + 3d_{E^*} d_\nu^2 + d_\nu^3,$$
$$c_6 = -12\beta d_E E_p(0)\pi_\nu + 3d_E^2 d_{E^*} + 4d_E d_{E^*}^2 + 18d_E d_{E^*} d_\nu - 4d_{E^*}^3 + 3d_{E^*} d_\nu^2,$$
$$c_7 = -2\beta d_E^3 E_p(0)\pi_\nu - 8\beta d_E^2 d_{E^*} E_p(0)\pi_\nu - 12\beta d_E^2 E_p(0) d_\nu\pi_\nu + 6\beta d_E d_{E^*}^2 E_p(0)\pi_\nu$$
$$+4\beta d_E d_{E^*} E_p(0) d_\nu\pi_\nu - 2\beta d_E E_p(0) d_\nu^2\pi_\nu + 3d_E^3 d_{E^*} d_\nu - d_E^2 d_{E^*}^2 + 3d_E^2 d_{E^*} d_\nu$$
$$+6d_E^2 d_{E^*} d_\nu^2 - d_E d_{E^*}^3 d_\nu + 2d_E d_{E^*}^2 d_\nu^2 + 3d_E d_{E^*} d_\nu^3 - d_{E^*}^3 d_\nu^2 - d_{E^*}^2 d_\nu^3,$$
$$c_8 = -3\beta d_E d_{E^*} E_p(0)\pi_\nu - 4\beta d_E E_p(0) d_\nu\pi_\nu - d_E^3 d_{E^*} - d_E^3 d_\nu - d_E^2 d_{E^*}^2 - 3d_E^2 d_{E^*} d_\nu$$
$$-2d_E^2 d_\nu^2 - d_E d_{E^*}^2 d_\nu - d_E d_{E^*} d_\nu^2 - d_E d_\nu^3 + d_{E^*}^2 d_\nu^2 + d_{E^*} d_\nu^3,$$
$$c_9 = -24\beta d_E E_p(0)\pi_\nu + 3d_E^2 d_{E^*} + 2d_E d_{E^*}^2 + 18d_E d_{E^*} d_\nu + 2d_{E^*}^2 d_\nu + 3d_{E^*} d_\nu^2,$$
$$c_{10} = 12\beta^2 d_E E_p(0)^2\pi_\nu^2 - 4\beta d_E^2 d_{E^*} E_p(0)\pi_\nu - 8\beta d_E d_{E^*}^2 E_p(0)\pi_\nu - 24\beta d_E d_{E^*} E_p(0) d_\nu\pi_\nu$$
$$-4\beta d_{E^*}^2 E_p(0) d_\nu\pi_\nu - 4\beta d_{E^*} E_p(0) d_\nu^2\pi_\nu + 3d_E^2 d_{E^*}^2 d_\nu + 2d_E d_{E^*}^3 d_\nu$$
$$+6d_E d_{E^*}^2 d_\nu^2 + 2d_{E^*}^3 d_\nu^2 + 3d_{E^*}^2 d_\nu^3,$$
$$c_{11} = d_E^2 E_p(0)\Big(\beta d_E^2 E_p(0)\pi_\nu + 6\beta d_E d_{E^*} E_p(0)\pi_\nu + 6\beta d_E E_p(0) d_\nu\pi_\nu + 2\beta d_{E^*} E_p(0) d_\nu\pi_\nu$$
$$+\beta E_p(0) d_\nu^2\pi_\nu - d_E^2 d_{E^*}^2 - 2d_E^2 d_{E^*} d_\nu - 4d_E d_{E^*}^2 d_\nu - 4d_E d_{E^*} d_\nu^2 - 3d_{E^*}^2 d_\nu^2 - 2d_{E^*} d_\nu^3\Big),$$

$$d_1 = \beta^2 d_{E^*}^3 \pi_v^2, \quad d_2 = \beta d_{E^*}^2 \pi_v \Big(-12\beta d_E E_p(0)\pi_v + d_E^2 d_{E^*} + 6 d_E d_{E^*} d_v + d_{E^*} d_v^2 \Big),$$

$$\begin{aligned} d_3 = {} & d_E d_{E^*} \Big(12\beta^2 d_E E_p(0)^2 \pi_v^2 - 2\beta d_E^2 d_{E^*} E_p(0)\pi_v - 12\beta d_E d_{E^*} E_p(0) d_v \pi_v \\ & -2\beta d_{E^*} E_p(0) d_v^2 \pi_v + d_E^2 d_{E^*}^2 d_v + 2 d_E d_{E^*}^2 d_v^2 + d_{E^*}^2 d_v^3 \Big), \end{aligned}$$

$$\begin{aligned} d_4 = {} & d_E^2 E_p(0) \Big(-4\beta^2 d_E E_p(0)^2 \pi_v^2 + \beta d_E^2 d_{E^*} E_p(0)\pi_v + 6\beta d_E d_{E^*} E_p(0) d_v \pi_v \\ & +\beta d_{E^*} E_p(0) d_v^2 \pi_v - d_E^2 d_{E^*}^2 d_v - 2 d_E d_{E^*}^2 d_v^2 - d_{E^*}^2 d_v^3 \Big) \end{aligned}$$

Equation (3) encompasses a composition of differential polynomials which undergo normalization. These polynomials intricately involve the state variables under observation and their respective derivatives. It is noteworthy that the coefficients within said polynomials exhibit rational functions contingent upon the parameters of the model. Now, we focus on acquiring the Gröbner basis (Boulier, 2007; Buchberger, 1998) from the coefficients of the input-output equation (3). First, we use DAISY to assign a set of numerical random points $\hat{p}$ in the parameter space, i.e, $\hat{p} = [d_E, \beta, d_{E^*}, \pi_v, d_v, E_p(0)] = [2,5,7,13,11,3]$. Using DAISY yields

$$\begin{aligned} & d_{E^*} - 7 = 0, \\ & d_E E_p(0) - 6 = 0, \\ & 2d_E - d_{E^*} + 2d_v - 19 = 0, \\ & d_{E^*}(d_E + d_{E^*} + d_v) - 140 = 0, \\ & d_E E_p(0)(3d_E + 2d_{E^*} + 3d_v) - 318 = 0, \\ & d_E + d_{E^*} + d_v - 20 = 0, \\ & \beta\pi_v - 65 = 0, \\ & d_E + 2d_{E^*} - 16 = 0. \end{aligned}$$

Hence, d_{E^*} is globally identifiable. Subsequently, after some algebraic manipulation, we derive the Gröbner basis of model (1) to be

$$d_E = 2, d_{E^*} = 7, d_v = 11, E_p(0) = 3, \beta\pi_v = 65. \tag{4}$$

Consequently, the parameters $d_E, d_{E^*}, d_v, E_p(0)$, and the combination of $\beta\pi_v$ in model (1) are structurally identifiable and the model parameters are not structurally identifiable if the infected epithelial cells are given. □

Theorem 2.3 posits that the global identification of the parameters pertaining to model (1) is unattainable through the available observations of infected epithelial cells. To elevate the level of parameter identifiability, a conventional method involves the fixation of specific parameters procured from alternative sources.

Remark 2.1. If the parameter β or π_v is fixed, then all parameters of model (1) are globally identifiable from the observations of infected epithelial cells.

Proof. This is a direct result from equation (4). □

Remark 2.2. If the virus load or all state variables are observable from external sources, then all parameters of the model (1) become globally identifiable.

Proof. Assuming that we insert an observation about the virus load level, denoted as $y_2 = v(t)$ in Theorem 2.3, we use DAISY again to derive the following input-output equation (5):

$$\begin{aligned} 0 = {} & \frac{dy_2}{dt} - y_1\pi_v + y_2 d_v, \\ 0 = {} & \left(\frac{dy_1}{dt}\right)^2 y_2 - \frac{dy_1}{dt} y_1 \pi_v + \frac{dy_1}{dt} y_2^2 \beta + \frac{dy_1}{dt} y_2 (d_E + d_{E^*} + d_v) - y_1^2 d_{E^*} \pi_v \\ & + y_1 y_2^2 \beta d_{E^*} + y_1 y_2 d_{E^*}(d_E + d_v) - y_2^2 \beta d_E E_p(0). \end{aligned} \tag{5}$$

If we set $\hat{p} = [d_E, \beta, d_{E^*}, \pi_v, d_v, E_p(0)] = [2,5,7,13,11,3]$ and use the known initial conditions of the model (1) as mentioned in the paragraph above in Theorem 2.3, then we obtain the Gröbner basis from (5) as below:

$$d_E = 2, \beta = 5, d_{E^*} = 7, \pi_v = 13, d_v = 11, E_p(0) = 3.$$

Therefore, all parameters of model (1) are globally identifiable.

If measured variables are all state variables, i.e. $y_1 = E_p^*(t)$, $y_2 = v(t)$, $y_3 = E_p(t)$. Then DAISY gives the input-output equations as follows

Table 1
Structural identifiability of system (1) under different observations.

Measured variable	Identifiable parameters
E_p^*	$\{d_E, d_{E^*}, d_v, E_p(0)\}$
v	$\{d_E, \beta, d_{E^*}, d_v\}$
E_p^* and v	$\{d_E, \beta, d_{E^*}, \pi_v, d_v, E_p(0)\}$
E_p^*, v and E_p	$\{d_E, \beta, d_{E^*}, \pi_v, d_v, E_p(0)\}$

$$\begin{aligned} 0 &= \frac{dy_1}{dt} + y_1 d_{E^*} - y_2 y_3 \beta, \\ 0 &= \frac{dy_2}{dt} - y_1 \pi_v + y_2 d_v, \\ 0 &= \frac{dy_3}{dt} + y_2 y_3 \beta + y_3 d_E - d_E E_p(0). \end{aligned} \tag{6}$$

Similarly, all parameters are structurally globally identifiable. □

Actually, the viral load data is acquired from Zheng et al. (Zheng et al., 2020). In this case, we have the following parameter identifiable outcome.

Remark 2.3. If the virus load level is known, the parameters of the model (1) are unidentifiable, more specifically, parameters π_v and $E_p(0)$ are inherently unidentifiable.

Proof. For simplicity, we represent $y_1(t) = v(t)$ and take $v(0) = 152.95$. Now, we apply the DAISY to derive the following input-output equation:

$$\begin{aligned} 0 = {} & \frac{d^3 y_1}{dt^3} y_1 - \frac{d^2 y_1}{dt^2}\frac{dy_1}{dt} + \beta \frac{d^2 y_1}{dt^2} y_1^2 + (d_E + d_{E^*} + d_v)\frac{d^2 y_1}{dt^2} y_1 - (d_{E^*} + d_v)\left(\frac{dy_1}{dt}\right)^2 \\ & + \beta(d_{E^*} + d_v)\frac{dy_1}{dt} y_1^2 + d_E(d_{E^*} + d_v)\frac{dy_1}{dt} y_1 + \beta d_{E^*} d_v y_1^3 + d_E\big(-\beta E_p(0)\pi_v + d_{E^*} d_v\big) y_1^2. \end{aligned} \tag{7}$$

Letting $\hat{p} = [d_E, \beta, d_{E^*}, \pi_v, d_v, E_p(0)] = [2, 5, 7, 13, 11, 3]$, we obtain the ultimate Gröbner basis as below

$$d_E = 2, \beta = 5, d_{E^*} = 7, d_v = 11, \pi_v E_p(0) = 39. \tag{8}$$

This indicates that parameters π_v and $E_p(0)$ have an infinite possibility satisfying the last equation of (8). Hence, the parameters in model (1) are not structurally identifiable based on the viral load level. □

From what has been discussed, we summarize the results of the identifiability analysis in Table 1.

3. Practical identifiability analysis of model (1)

The structural identifiability analysis presents identifiable parameters and parameter combinations from the observed noise-free data. In reality, epidemiological data frequently exhibits inherent disturbances, being obtained at discrete moments in time. The concept of practical identifiability encompasses not only the quantity and quality of the collected data, but also takes into account their diverse noise levels. Therefore, conducting the practical identifiability analysis holds paramount importance in discerning the model parameters. The outcomes of practical identifiability may diverge from the findings of the previously structural identifiability.

Table 2
Fitted parameter values of system (1).

Parameters	E_p^*		v		E_p^* and v	
	Value	Range	Value	Range	Value	Range
d_E	0.19	0–1	0.02	0–1	1.50	0–10
β	0.09	0–1	0.0012	0–20	2.95	0–100
d_{E^*}	0.46	0–1	0.11	0–100	0.19	0–1000
π_v	0.48	0–1	4.08	0–25	26.57	0–1000
d_v	1.02	1–10	0.3	0–100	0.69	0–100
$E_p(0)$	26.9	20–30	42.7	1–80	1.00	1–1000
$E_p^*(0)$	2.59	Li et al. (2020b)	4.0	2–50	2.59	Li et al. (2020b)

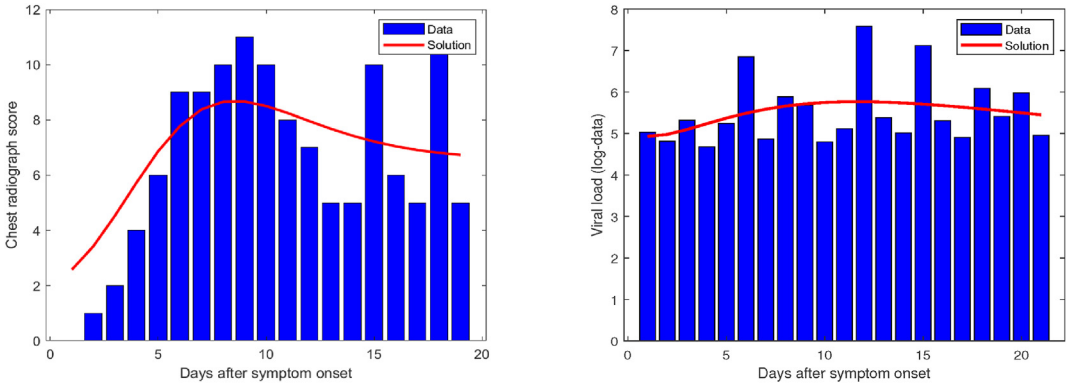

(a) Fitting curve of infected cells E_p^*. (b) Fitting curve of viral load v.

Fig. 1. The chest radiograph score data and viral load data (blue bars) and the associated solution to model (1) (red curves) with the estimated values presented in Table 2.

3.1. Parameters estimation

To assess practical identifiability, we initially estimate the parameters $p = [d_E, E_p(0), \beta, d_{E^*}, \pi_v, d_v]$ of model (1) through the resolution of the constrained optimization problem (9) which minimizing the following objective, i.e. residual sum of squares (rss):

$$rss = \sum_{i=1}^{n} (y(t_i) - Y^i)^2 \tag{9}$$

where $\{(t_1, Y^1), (t_2, Y^2), \ldots, (t_n, Y^n)\}$ denote the chest radiograph scores (Li et al., 2020b) or the virus load data (Zheng et al., 2020) at each discrete time $t_j (j = 1, 2, \ldots, n)$, and $\{y(t_1), y(t_2), \ldots, y(t_n)\}$ represents the solution of model (1). Obviously,the residual sum of squares (rss) is a function about the parameters of model (1). To address such optimal control problem, we employ *fminsearchbnd* in MATLAB with specified lower and upper bounds to estimate the parameter values through the least-square approach. For the data set v, we logarithmically transform them to reduce their dimensionality. And meanwhile the initial value $E_p^*(0)$ of infected cells is considered as an estimated parameter for repeated optimization iteration. The optimal values for the parameters are presented in Table 2. The columns showcase estimated parameters when known infected cells, viral load and these two sets of data are simultaneously known. Fig. 1 and Fig. 2 depict the mimic results of the data set and the associated solution to model (1).

3.2. Practical identifiability analysis

A parameter that possesses structural identifiability may be rendered practically unidentifiable owing to the absence of data devoid of noise. To further scrutinize the parameter identifiability of model (1), we implement the Monte Carlo Simulations (MCS) to take the practically identifiable analysis of the model parameters. Monte Carlo Simulations evaluate a set of scenarios involving varying known observations with different noise levels. We initiate Monte Carlo simulations by establishing the presumed parameters stipulated in Table 2 as the veritable values $\hat{p}$. Subsequently, we fabricate $M = 1000$ arrays of

Table 3
Specific steps for MCS.

1. Solve the mathematical model (1) numerically with the genuine parameters $\hat{p}$ and obtain the output vector $g(x(t_i), \hat{p})$ at discrete temporal instances $\{t_i\}_{i=1}^n$.
2. Add noise level to the output vector $g(x(t_i), \hat{p})$ obtained from step 1 and generate 1000 groups of simulated data.
3. Fit the model (1) to each of the meticulously crafted simulated data by solving the optimization problem (9) to assess a robust estimation of the parameter set p_j for $j = 1, 2, \ldots, 1000$.
4. Calculate the average relative estimation errors for each parameter in the parameter set of p.
5. Repeat the aforementioned steps 1–4 with gradually amplifying noise levels of $\sigma_0 = 0, 1, 5, 10, 20\%$, respectively.

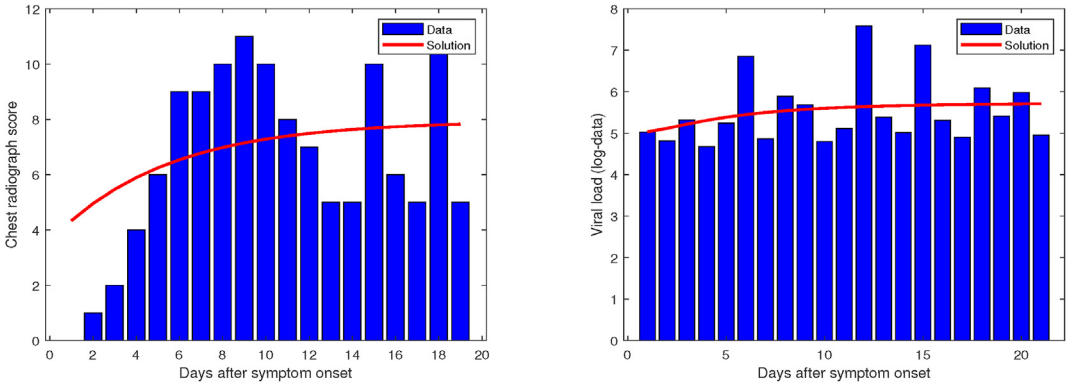

Fig. 2. The snapshots of the fitting results with E_p^* and $v(t)$

fabricated data by introducing diverse degrees of perturbation to the recorded observations of infected cells E_p^* and the SARS-CoV-2 virus load v. The Monte Carlo simulations are executed employing two distinct distribution frameworks: Gaussian distribution and Poisson distribution. The intricate mechanics of the Monte Carlo simulation algorithm are delineated in Table 3.

Next, we will present some supplements. A thousand of simulated data come from the

$$y_i = g(x(t_i), \hat{p}) + g(x(t_i), \hat{p})^f \epsilon_i, \tag{10}$$

where $g(x(t_i), \hat{p})^f \epsilon_i$ represents the measurement errors with $f \geq 0$.

(i) Gaussian distribution: ϵ_i, which is assumed to be independent, identically distributed random variable with a zero mean and a finite variance of σ_0^2 at a given error. We draw samples from the Gaussian distribution with a mean equal to the result vector acquired in the initial step, and a standard deviation of σ_0% of the mean value. In this scenario, we establish $f = 1$ in equation (10) and subsequently generate the artificial dataset by extracting samples from the Gaussian distribution as below

$$y_i = g(x(t_i), \hat{p}) + g(x(t_i), \hat{p})\epsilon_i,$$

where $Var(\epsilon_i) = \sigma_0^2$. Hence, the variables y_i have mean $E(y_i) = g(x(t_i), \hat{p})$ and variances $Var(y_i) = g(x(t_i), \hat{p})^2\sigma_0^2$. In Fig. 3, we give a series of plots of the number of synthetic cells or SARS-CoV-2 viruses with different noise levels σ_0.

(ii) Poisson distribution: Assume the stochastic variables y_i have $E(y_i) = Var(y_i) = g(x(t_i), \hat{p})$. Fig. 4 depicts the artificial data produced by perturbing a poisson distribution. Comparing Figs. 1-2 and Fig. 3, we can see that the actual data contain an approximately 20% Gaussian distribution error.

According to (Miao et al., 2011), the average relative estimation errors for each parameter is calculated by

$$ARE(p^{(k)}) = 100\% \frac{1}{M} \sum_{j=1}^{M} \frac{\left|\widehat{p}^{(k)} - p_j^{(k)}\right|}{\widehat{p}^{(k)}}, \tag{11}$$

where $p^{(k)}$ represents the kth parameter in the set p. Similarly, $\hat{p}^{(k)}$ is the kth parameter in the true parameter set $\hat{p}$, while $p_j^{(k)}$ represents the kth parameter in the estimated parameter set p_j.

Applying (11), Tables 4–6 give the average relative estimation errors of the parameters with Gaussian distribution for each output and noise level. Table 7 gives the average relative estimation errors of all parameters with a poisson distribution for two data sets. The values of average relative estimation errors provide significant insights into the practical identifiability of the parameters of the model (1). As expected, amplifying the auditory disturbance within a dataset leads to a concomitant augmentation of the magnitudes of average relative estimation errors. We have noticed that the values of β and π_v of average relative estimation errors in Table 4 are much more sensitive to the variation of data noise consistence with the consequence of structurally identifiable analysis. When $\sigma_0 = 20\%$, the parameters d_E and d_v also exhibit significant large absolute average relative estimation errors, indicating that these two parameters are unidentifiable as well. The remaining parameters values of average relative estimation errors exhibit small changes in magnitude compared with above parameters and fall in a relatively reasonable range and so they are practically identifiable.

In order to gain a clear understanding of the identifiable outcomes, we plot the rss in each parameter of model (1) with a local range and the values of the remaining parameters fixed in Table 2. As we know, a slightly flat graph of the plot signifies the unidentifiability of the parameter. By examining the vertical axis of Fig. 5, we can once again observe that, apart from the

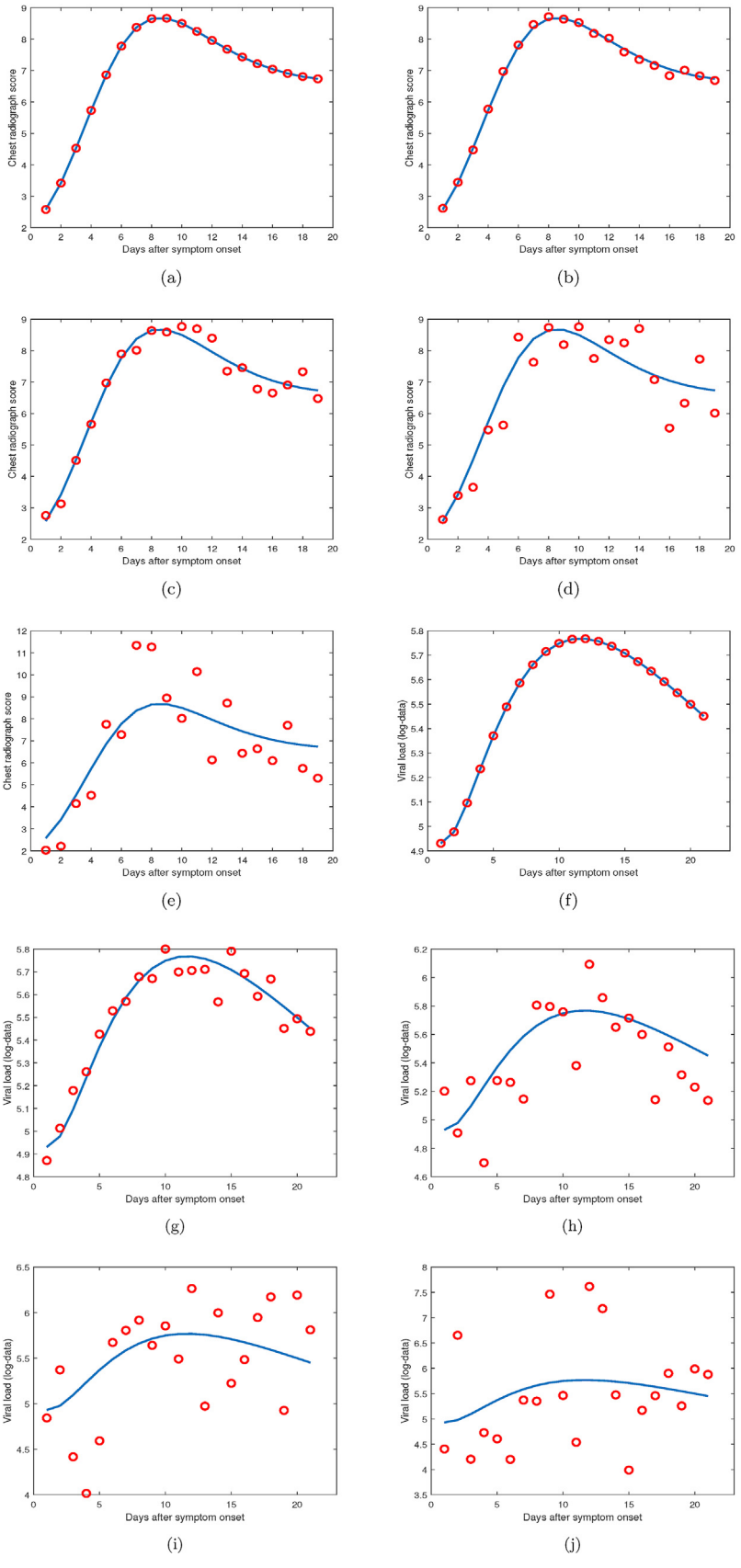

Fig. 3. (a)–(e): The plot scenarios of the data E_p^* generated by Gaussian distributions for each error. (f)–(j): The plot scenarios of the data v generated by similar processes as in (a)–(e). Figure (a) and (f) with a noise level of $\sigma_0 = 0\%$, (b) and (g) with a noise level of $\sigma_0 = 1\%$, (c) and (h) with a noise level of $\sigma_0 = 5\%$, (d) and (i) with a noise level of $\sigma_0 = 10\%$ and (e) and (j) with a noise level of $\sigma_0 = 20\%$.

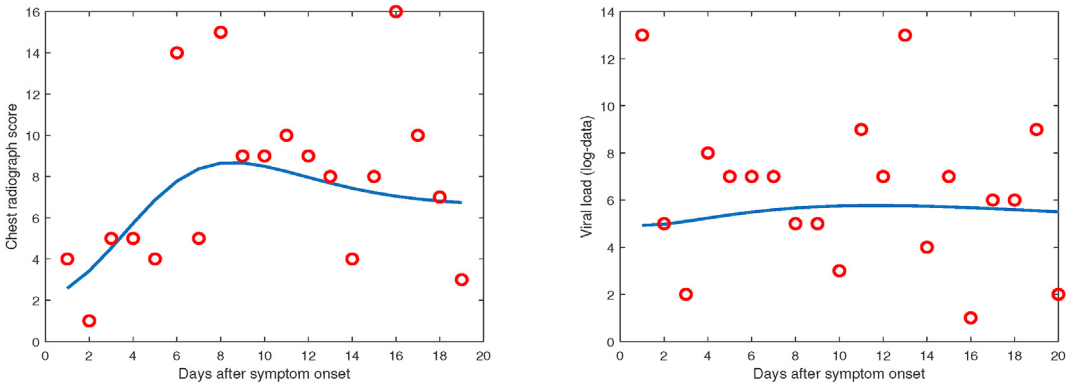

Fig. 4. Synthetic data sets of E_p^* and v generated by a poisson distribution

substantial variation range of (c) and (f), the changes in rss for the remaining four parameters are minimal comparing (c) and (f). This finding further validates the results presented in Table 4.

To reveal the identifiability of parameters β and π_v, we plot a contour graphic and the rss in the $\beta - \pi_v$ parameter space by fixing other parameters in Table 2 (see Fig. 6). As shown in Fig. 6(a), the contour plot of β and π_v extends infinitely without an intersection and it consistently aligns with the previous results.

To assess the parameters identifiability of the observable data v, we have conducted a similar procedure to the one used as data E_p^*. We calculate the average relative estimation errors listed in Table 5, where true parameters are chosen from Table 2. Firstly, in the context of structure identification (Remark 2.3), the statement suggests that the parameters π_v and $E_p(0)$ are practically unidentifiable. The investigation of structure identification is conducted under the assumption of noise-free data. Therefore, if certain parameters are deemed structurally unidentifiable, they are likely to be practically unidentifiable as well.

Table 4
Average relative errors of model parameters with known E_p^* (Gaussian Distribution).

Parameters	$\sigma_0 = 0\%$	$\sigma_0 = 1\%$	$\sigma_0 = 5\%$	$\sigma_0 = 10\%$	$\sigma_0 = 20\%$
d_E	0	3.7	12.9	25.1	50.5
β	0	10.9	18.2	29.1	51.5
d_{E^*}	0	6.7	14.9	22.7	35.3
π_v	0	12.5	22.3	30.1	41.3
d_v	0	3.8	9.1	21.3	60.6
$E_p(0)$	0	6.3	10.7	11.7	11.8

Table 5
Average relative errors of model parameters with known v (Gaussian Distribution).

Parameters	$\sigma_0 = 0\%$	$\sigma_0 = 1\%$	$\sigma_0 = 5\%$	$\sigma_0 = 10\%$	$\sigma_0 = 20\%$
d_E	0	72.7	146.3	198.2	351.4
β	0	24.0	3918.2	14704.3	59996.4
d_{E^*}	0	42.0	81.4	103.7	154.3
π_v	0	39.8	85.2	143.8	226.9
d_v	0	44.6	115.8	248.3	467.1
$E_p(0)$	0	29.0	49.4	58.0	63.0

Table 6
Average relative errors of model parameters with known two datasets (Gaussian Distribution).

Parameters	$\sigma_0 = 0\%$	$\sigma_0 = 1\%$	$\sigma_0 = 5\%$	$\sigma_0 = 10\%$	$\sigma_0 = 20\%$
d_E	0	1.8	10.1	20.2	36.1
β	0	81.2	145.8	202.7	214.1
d_{E^*}	0	2.0	10.7	23.0	48.2
π_v	0	11.3	54.8	101.3	147.8
d_v	0	11.9	58.6	106.4	154.4
$E_p(0)$	0	0.3	3.2	9.5	22.2

Table 7
Average relative errors of model parameters with a poisson distribution.

Parameters	d_E	β	d_{E^*}	π_v	d_v	$E_p(0)$
E_p^*	65.8	114.9	48.6	50.5	153.3	17.1
v	758.3	88544.6	818.1	336.2	541.5	63.2
E_p^* and v	55.6	260.1	189.6	264.2	273.7	168.2

There is a visualization in Fig. 7 that supports the conclusion of the unidentifiability of π_v and $E_p(0)$. We have noted that the average relative estimation errors of β are relatively large and hence β is practically unidentifiable. As shown in Fig. 7 (b), the scenario of rss in β looks flat and this further illustrates the unidentifiability of β. Additionally, the average relative estimation

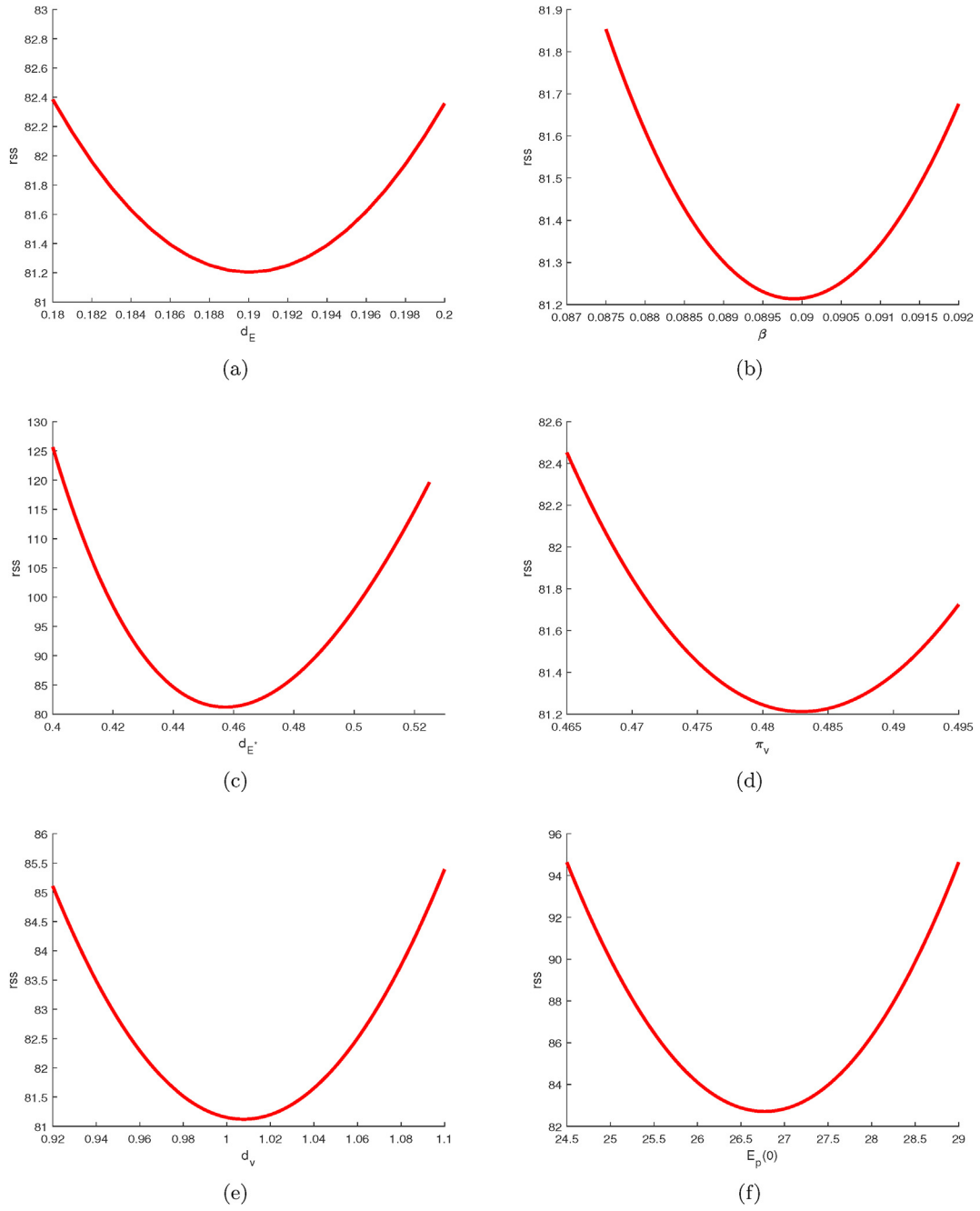

Fig. 5. The scenarios of rss in each parameters with known values of E_p^*.

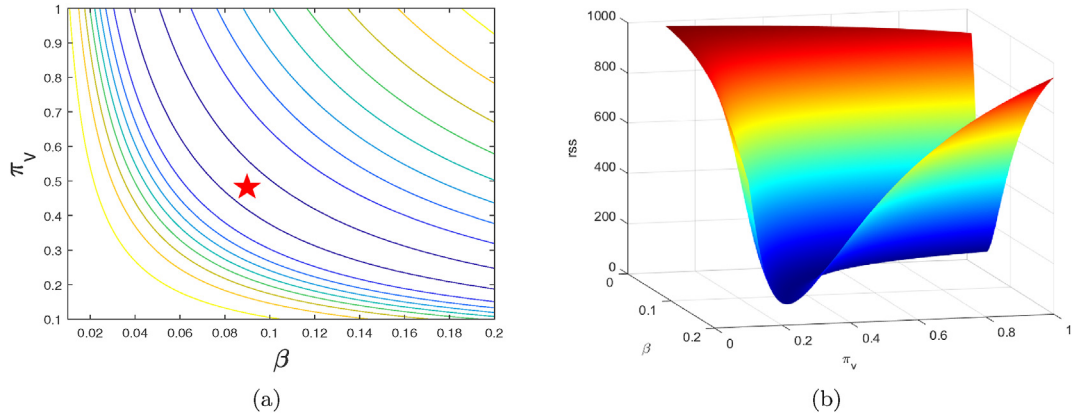

Fig. 6. The scenarios of rss in $\beta - \pi_v$ parameter space. (a) The contour plot of rss. (b) The surf of rss.

errors of d_v and d_E are roughly high when the noise level is taken as $\sigma_0 = 1\%$. Fig. 7 (e) and (a) display that the snapshots of rss in d_v and d_E have a small magnitude in a certain range and hence they are also unidentifiable. It can be observed that all parameters, except for β, can be considered as practically unidentifiable, because their rss values fluctuate only by a few tenths from Fig. 6.

From Remark 2.2, we have known that system (1) is structurally identifiable if $E_p^*(t)$ and $v(t)$ are observable. Now, we detect whether it is practically identifiable with two available sets of E_p^* and v. Similar to the mentioned above, we calculate the AREs in Table 6 and find that parameter β is practically unidentifiable. Moreover, it follows from Table 6 that the average relative estimation errors of parameters π_v and d_v are much larger than those values of other parameters for each noise level. This indicates that π_v and d_v are practically unidentifiable, while other parameters are relatively identifiable. Hence, in clinical trials, it is crucial to prioritize and direct attention towards investigating the transmission rate, replication rate and mortality rate of the virus. As previously conducted, we have additionally constructed visual representations of the residual sum of squares (rss) corresponding to each parameter. From Fig. 8, it is evident that the identifiability of β remains elusive. Furthermore, Fig. 8 (d) and (e) substantiate the profound unidentifiability of π_v and d_v.

To deeply insight into the parameter identifiability, we compute the AREs in Table 7 with a poisson error and a mean of $g(x(t_i), \hat{p})$. The observation has shown that parameters β and d_v exhibit notably higher values of ARE as the observable data sets of infected cells. Nevertheless, when the viral load is known, it appears that the average relative errors of parameters β is relatively high. Therefore, from Tables 4–7, it is evident that the parameters with higher average relative estimation errors remain consistent irrespective of the data sets perturbing by a Gaussian or a poisson distribution.

4. Impact of parameters on epidemic quantities

Sensitive analysis (SA) of epidemiological parameters allows policy-makers to determine which parameter takes a significant impact on the concerned quantity. According to Lemma 1.1, it is established that the basic reproduction number R_0 plays a crucial role in determining the persistence of the SARS-CoV-2 infection. The severity of an infection within a host can be assessed by evaluating the final size of both infected cells and the SARS-CoV-2 virus. Hence, we conduct the SA of the epidemiological quantities, such as the reproduction number R_0, infected cells $\overline{E_p^*}$ and virus load $\bar{v}$ with respect to the parameters of model (1).

4.1. Elasticity analysis

The elasticity of quantity Q with respect to parameter p can be elegantly formulated as follows

$$\gamma_p^Q = \frac{\partial Q}{\partial p} \times \frac{p}{Q}. \tag{12}$$

The elasticity represents 1% changes in parameter p will cause $\gamma_p^Q\%$ in quantity Q. $\gamma_p^Q > 0$ implies that Q increases with p while $\gamma_p^Q < 0$ means that Q decreases when p increases. The results of elasticities provide useful information on the sensitivity of the quantity of interest to various parameters and it is helpful for policy-makers to devise corresponding control strategies to mitigate the disease prevalence.

We first consider the elasticities $\gamma_p^{R_0}$ of the basic reproduction number of R_0. From (12), we have that

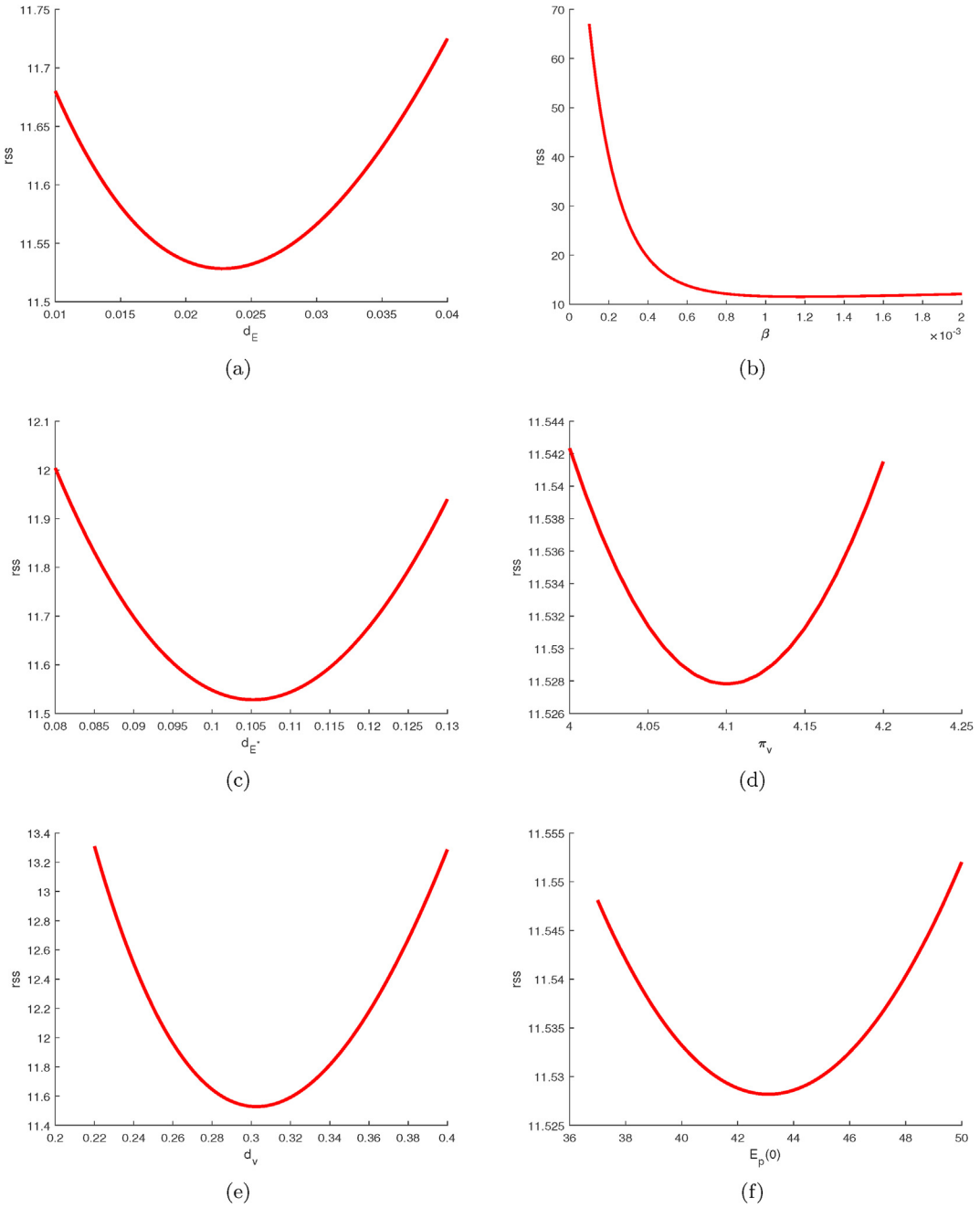

Fig. 7. The scenarios of rss in each parameters with known values of v.

$$\gamma_{\beta}^{R_0} = \gamma_{\pi_v}^{R_0} = \gamma_{E_p(0)}^{R_0} = 1,$$
$$\gamma_{d_{E^*}}^{R_0} = \gamma_{d_v}^{R_0} = -1.$$

The above results reveal that the parameters $\beta, \pi_v, E_p(0), d_{E^*}, d_v$ exert nearly identical levels of influence on R_0. Additionally, R_0 has demonstrated an upward trend concomitant with the escalation in the infection rate β, the release rate of the virus π_v, and

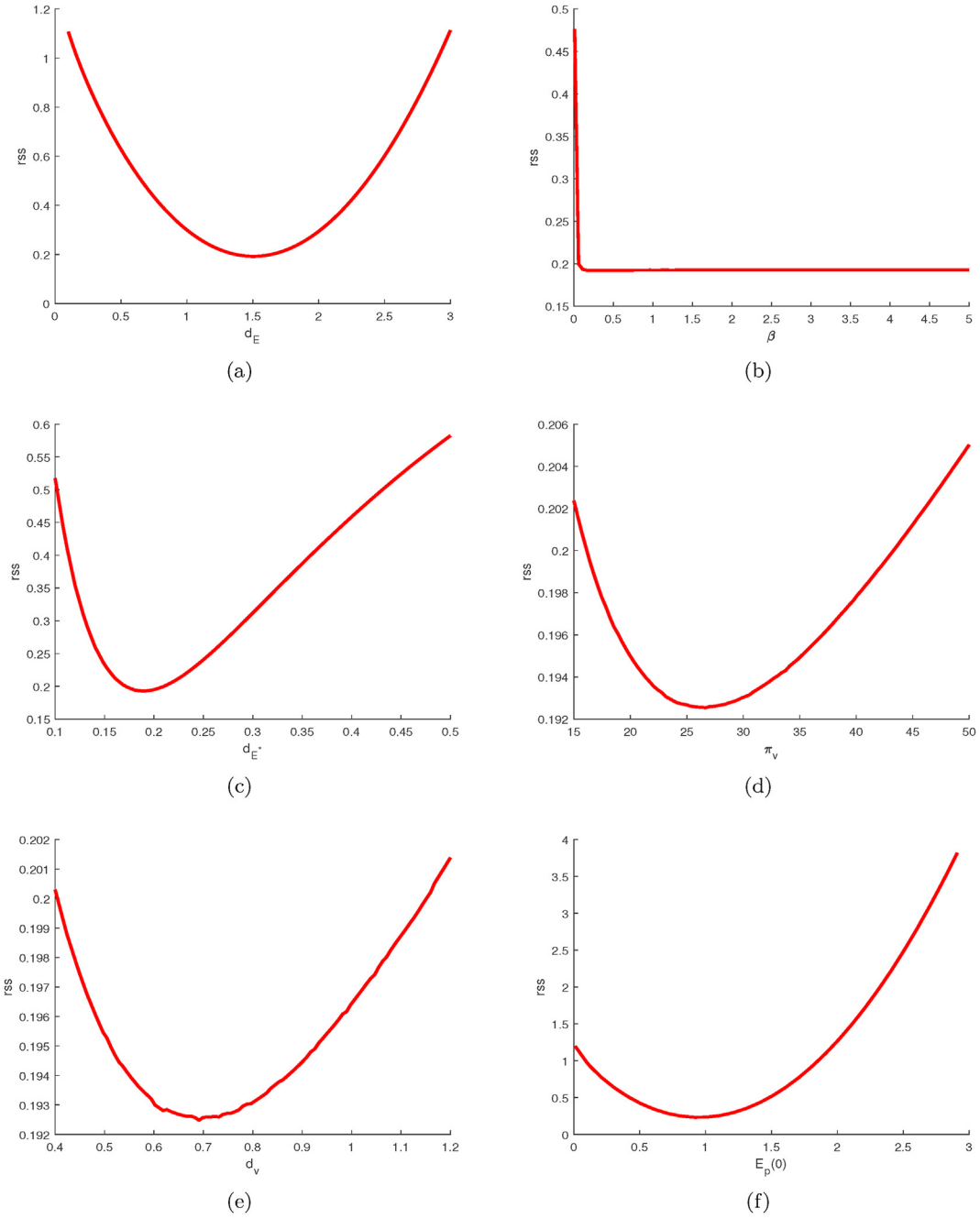

Fig. 8. The scenarios of rss in each parameters with known two datasets.

the initial quantity of uninfected epithelial cells $E_p(0)$. Conversely, it has exhibited a negative correlation with the simultaneous increase in the death rate d_{E^*} of infected epithelial cells and the decay rate d_v of the SARS-CoV-2 virus.

Similarly, we evaluate the influence of parameters on the eventual epidemic outcome by examining the elasticities of the endemic infected cells $\overline{E_p^*}$ and virus load $\bar{v}$ as quantities of interest, which are given in Section 1. The corresponding elasticities are derived as follows:

$$\gamma_{d_E}^{\overline{E_p^*}} = 1,$$

$$\gamma_{\beta}^{\overline{E_p^*}} = \frac{d_v d_{E^*}}{\beta\pi_v E_p(0) - d_v d_{E^*}} = \frac{1}{R_0 - 1},$$

$$\gamma_{\pi_v}^{\overline{E_p^*}} = \frac{d_v d_{E^*}}{\beta\pi_v E_p(0) - d_v d_{E^*}} = \frac{1}{R_0 - 1},$$

$$\gamma_{d_v}^{\overline{E_p^*}} = -\frac{d_v d_{E^*}}{\beta\pi_v E_p(0) - d_v d_{E^*}} = -\frac{1}{R_0 - 1},$$

$$\gamma_{d_{E^*}}^{\overline{E_p^*}} = -\frac{d_E E_p(0)\beta\pi_v}{d_E E_p(0)\beta\pi_v - d_E d_v d_{E^*}} = -\frac{1}{1 - \frac{1}{R_0}},$$

$$\gamma_{E_p(0)}^{\overline{E_p^*}} = \frac{E_p(0)\beta\pi_v}{E_p(0)\beta\pi_v - d_v d_{E^*}} = \frac{1}{1 - \frac{1}{R_0}}.$$

$$\gamma_{d_E}^{\overline{v}} = 1,$$

$$\gamma_{\beta}^{\overline{v}} = \frac{d_v d_{E^*}}{\beta\pi_v E_p(0) - d_v d_{E^*}} = \frac{1}{R_0 - 1},$$

$$\gamma_{\pi_v}^{\overline{v}} = \frac{\beta\pi_v d_E E_p(0)}{\beta\pi_v d_E E_p(0) - d_E d_v d_{E^*}} = \frac{1}{1 - \frac{1}{R_0}},$$

$$\gamma_{E_p(0)}^{\overline{v}} = \frac{E_p(0)\beta\pi_v}{E_p(0)\beta\pi_v - d_v d_{E^*}} = \frac{1}{1 - \frac{1}{R_0}},$$

$$\gamma_{d_{E^*}}^{\overline{v}} = -\frac{d_E E_p(0)\beta\pi_v}{d_E E_p(0)\beta\pi_v - d_E d_v d_{E^*}} = -\frac{1}{1 - \frac{1}{R_0}},$$

$$\gamma_{d_v}^{\overline{v}} = -\frac{\beta\pi_v d_E E_p(0)}{\beta\pi_v d_E E_p(0) - d_E d_v d_{E^*}} = -\frac{1}{1 - \frac{1}{R_0}}.$$

Utilize the baseline parameter values respectively in Table 2, the elasticities of infected cells E_p^* and virus load v are given in Table 8. The second row of Table 8 suggests that the mortality rates of infected epithelial cells and the initial number of uninfected epithelial cells have the most significant impact on E_p^*. This observation implies that the direct administration of medications eradicates both healthy and infected cells, potentially serving as a crucial factor in reducing the prevalence of infected cells. Vaccination can activate the immune system, triggering the production of antibodies to combat SARS-Cov-2 viral infections. It also activates immune cells, further enhancing the immune response to SARS-Cov-2 virus. This immune reaction not only protects the vaccinated individual from severe infection but also reduces the severity of the disease and the risk of COVID-19 transmission.

The third row of Table 8 shows the replication rate of viruses π_v and the initial number of uninfected cells $E_p(0)$ have the greatest influence on the ultimate magnitude of SARS-Cov-2 virus v. Meanwhile, the death rate d_{E^*} of infected epithelial cells and the decay rate d_v of the virus have a significantly negative effect on the size of the endemic equilibrium of v. Quercetin Phytosome (QP), identified as a potential antiviral drug, has been found in clinical trials in the early stages of COVID-19 to be a potent antioxidant that scour free radicals well. Moreover, QP accelerates the clearance of the virus, leading to a quicker conversion of molecular test from positive to negative (Pierro et al., 2021). Simultaneously, it diminishes the severity of symptoms. The RNA-dependent RNA polymerases (RdRp) inhibitors, such as Remdesivir (Eastman et al., 2020) and Azvudine (Yu and Chang, 2022), effectively halt the replication of SARS-Cov-2 virus during reverse transcription. Hence, the implement of Ambasvirumab and Romisevirumab serves to inhibit the binding of the SARS-Cov-2 virus to target cells, thereby preventing the invasion of SARS-CoV-2 virus in an individual (Shan et al., 2022).

Table 8
The elasticities γ_p^Q of R_0, $\overline{E_p^*}$ and $\overline{v}$ with respect to parameter values of model (1).

Parameters	d_E	β	d_{E^*}	π_v	d_v	$E_p(0)$
$\gamma_{R_0}^{R_0}$	0	1	−1	1	−1	1
$\gamma_{\overline{E_p^*}}^{\overline{E_p^*}}$	1	0.7	−1.7	0.7	−0.7	1.7
$\gamma_{\overline{v}}^{\overline{v}}$	1	0.2	−1.2	1.2	−1.2	1.2

4.2. Dynamical sensitivity analysis

Latin hypercube sampling/partial rank correlation coefficient(LHS/PRCC) sensitivity analysis aims to identify crucial parameters that introduce uncertainty in predictions, and prioritize these parameters based on their significance in contributing to this uncertainty. In the realm of sensitivity analysis within the framework of LHS/PRCC, paramount importance is assigned to parameters showcasing substantial PRCC values, surpassing the threshold of 0.2 or descending below −0.2, along with the concomitant manifestation of minuscule p-values, breaching the boundary of 0.05. These parameters, deemed as the epitome of significance, occupy a pivotal role in the evaluation process. These parameters have a strong correlation with the output of interest, indicating their high importance in influencing the prediction imprecision. By identifying and prioritizing these parameters, analysts can focus on reducing the uncertainties associated with them to improve the overall accuracy and reliability of the predictions.

Fig. 9 displays the temporal variation of PRCC values for each model parameter. The shaded gray region in Fig. 9 represents parameters that have negligible influence on the dynamic process. This figure visualizes the sensitivity of these parameters to both E_p^* and v at each moment, allowing us to observe how this sensitivity changes as the dynamics of system (1) evolves. As shown in Fig. 9 (a), the parameters d_E, β, π_v and $E_p(0)$ positively impact the evolution of infected cells $E_p^*(t)$, while d_v and d_{E^*} have a negative influence. Specifically, the propagation of infected cells during the initial ten days is predominantly influenced by the transmission rate β. This can be effectively achieved by impeding the interaction between the S protein presented on the viral surface and the ACE2 receptor located on host cells within the first ten days of the infectious period (Al-Darabsah et al., 2023; Taylor et al., 2021). Moreover, the effect of d_E on the size of infected cells E_p^* increases significantly during the initial ten days and subsequently becomes the dominant factor influencing the size of infected cells E_p^*. Hence, reducing the rate d_E of decay in healthy cells is effective in reducing the size of infected cells E_p^*. The mortality rate d_{E^*} of infected cells and d_v of viral burden exert a substantial detrimental influence on the proliferation of afflicted cellular collectives. Indeed, antiviral drugs like remdesivir and lopinavir/ritonavir have been used in the treatment of COVID-19 to reduce the duration of infection and limit viral replication (Gordon et al., 2020; Liu and Wang, 2020; Sanders et al., 2020).

Conversely, the transmission rate β has the profound impact on the proliferation of the SARS-Cov-2 virus $v(t)$ initially but diminishes and levels off over time in Fig. 9 (b). Additionally, the death rate d_v of viruses and the decay rate d_{E^*} of infected cells have substantial influence on the multiplication of the $v(t)$ at any given moment. This finding, combined with the results of the sensitivity analysis depicted in Fig. 9 (a), suggests that accelerating the death of the SARS-CoV-2 virus and decreasing the duration of infectiousness would be more effective in mitigating COVID-19 infections within a host. Absolutely, inhibiting viral replication is a crucial strategy in controlling the spread of infection and potentially reducing the severity of symptoms.

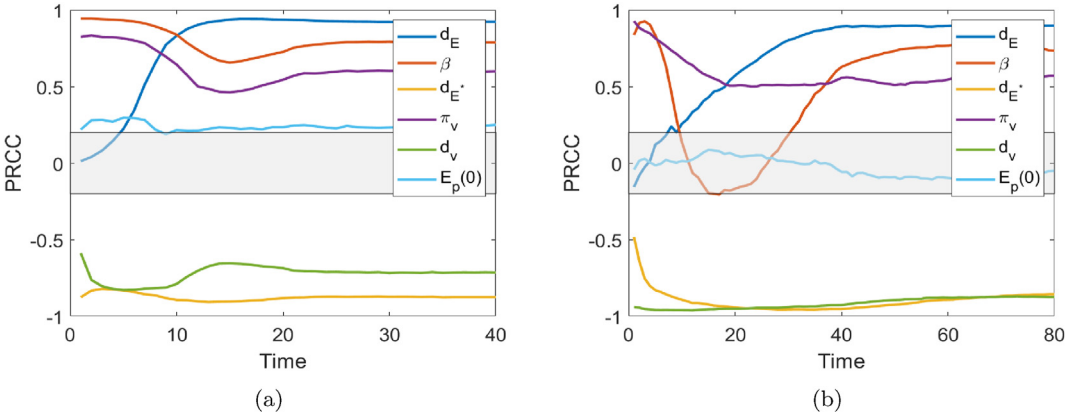

Fig. 9. The dynamical PRCC values of sensitivity analysis. (a)The dynamical PRCC values of infected cells $E_p^*(t)$; (b)The dynamical PRCC values of SARS-cov-2 virus $v(t)$.

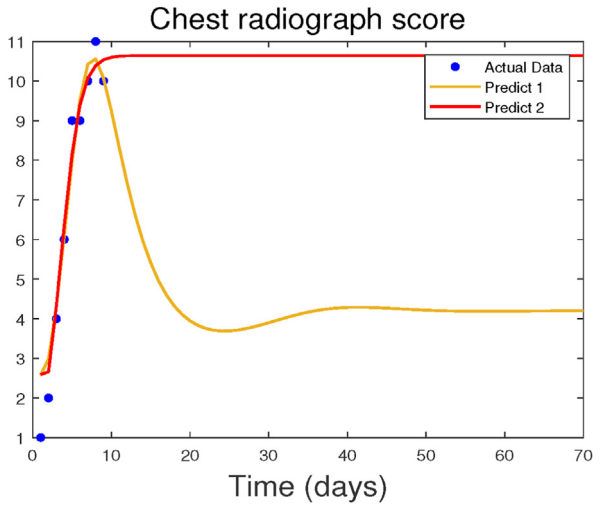

Fig. 10. The significance of parameter identifiability.

These control measures by targeting specific enzymes or proteins are essential for the replication of the virus. It appears that the impact of the parameters on infected cells (Fig. 9 (a)) and viruses (Fig. 9 (b)) was approximately similar at last, leading to comparable final results.

5. Discussion

The parameter identifiability of infectious disease models is a complex and important issue that needs to be considered comprehensively, taking into account factors such as data quality, parameter uniqueness, and determinacy. Parameter identifiability refers to the ability to uniquely estimate model parameters through observed data. In infectious disease models, the presence or absence of parameter identifiability directly affects our understanding of the behavior of infectious disease systems and the accuracy of our predictions. In this paper, we adopted DAISY to find the Gröbner basis and gave clear outcomes for the parameter structural identifiability of system (1) with noise-free data. Through the Monte Carlo experiments, we calculated the values of average relative estimation errors for detecting the parameter practical identifiability of system (1) with data perturbing by different types of Gaussian and Poisson noises. We found that the parameters are unidentifiable if we have either the number of infected pulmonary epithelial cells $E_p^*(t)$ or the SARS-Cov-2 virus load $v(t)$. More specifically, if we measured the number of infected pulmonary epithelial cells $E_p^*(t)$, model parameters could be identifiable except the infection rate β and the release rate π_v of SARS-Cov-2 virus. We also demonstrated that all parameters are identifiable if both the infected cells and the virus load data are known or the three state variables are observable. However, if one could ascertain solely the viral load of the SARS-Cov-2 virus, the unidentifiable parameters encompass the discharge rate π_v of the virus and the initial value $E_p(0)$ of uninfected cells, whereas the remaining parameters are identifiable. Those results are consistent with the outcomes of parameter structural identifiability.

Through a dynamic sensitivity analysis in detail, we have found that the transmission rate of β and the death rate d_{E^*} of infected cells play consequential roles in mitigating the SARS-Cov-2 infection. While the impact of d_E is indeed significant, it is not considered a feasible approach to kill healthy cells in clinical trials. Currently, some antiviral drugs such as remdesivir and lopinavir/ritonavir have been used in the treatment of COVID-19. These drugs can interfere with the virus replication process (reducing the value of β), thereby alleviating symptoms or shortening the course of the disease, i.e, increasing the value of d_{E^*}. In addition, other antiviral drugs are also being tested in clinical trials. Moreover, immunomodulatory drugs such as glucocorticoids are used to control inflammation and reduce the occurrence of related complications. Lemma 1.1 suggests that the basic reproduction number R_0 is a key value determining its long-term behaviors (Nath et al., 2021). According to fitting results in Section 3.2, the basic reproduction number R_0 was estimated either 2.5 or 6.4 from the observable data set of infected cells or SARS-Cov-2 virus load, respectively. While the value of $R_0 = 3.79$ as estimated in (Li et al., 2020b), the primary factor contributing to the difference was the variations in parameter values due to the practical unidentifiability (see Fig. 10). This emphasizes the significance of investigating the identifiability of parameters. As depicted in Fig. 10, both sets of parameter estimates yield a satisfactory fitting effect in the case of existing data. However, the prediction of infected cells in the body differs significantly: one set indicates a gradual decrease, while the other suggests a sustained high level. Once we determine the identifiability of parameters, it is crucial to focus on those that are non-identifiable. These parameters tend to be highly sensitive to changes in the system's output and require special attention.

There are some limitations in this paper. The first one is that the observed data came from some published paper. In particular, the data of the SARS-Cov-2 virus load were captured in (Zheng et al., 2020) using the *Grabit* package of MATLAB. It is undoubtable that there are some certain margin of errors as extracting data from the observable figures. The second one is that model (1) is directly employed from that in (Li et al., 2020b) and (Nath et al., 2021), which ignores the interaction between the SARS-Cov-2 virus and immune system response and it represents a consequential mechanism for the mitigation of SARS-Cov-2 infection within a host. Ultimately, the intricate interplay between the SARS-Cov-2 virus and the immune system, and the ensuing trade-offs, exert a pivotal influence on the dynamics of transmission at the population level, underscoring the crucial role they play in devising efficacious control measures. We will continue these topics in the future.

Author contributors

JY: Conceptualization, Methodology, Writing-original draft; SW: Data curation, Methodology, Software and Writing-original draft; XL: Writing-review & editing; XW: Funding Acquisition and Writing-review & editing; XZ,LH: epidemiological investigations, data curation.

Data and material availability

The data that supported this article may be available upon reasonable request to the corresponding author.

CRediT authorship contribution statement

Junyuan Yang: Writing – original draft, Methodology, Conceptualization. **Sijin Wu:** Writing – original draft, Software, Methodology, Data curation. **Xuezhi Li:** Writing – review & editing. **Xiaoyan Wang:** Writing – review & editing, Funding acquisition. **Xue-Song Zhang:** Data curation, Investigation. **Lu Hou:** Data curation, Investigation.

Declaration of competing interest

The authors declare that they have no known competing financial interests or personal relationships that could have appeared to influence the work reported in this paper.

Acknowledgements

This work is partially supported by Humanities and Social Foundation of Ministry of Education of China (22YJAZH129), the National Natural Science Foundation of China (No.12271143, No.61573016), the Shanxi Province Science Foundation (No. 20210302123454) and Shanxi Scholarship Council of China (2023–024).

References

Al-Darabsah, I., Liao, K. L., & Portet, S. (2023). A simple in-host model for COVID-19 with treatments: Model prediction and calibration. *Journal of Mathematical Biology, 86*(2), 20.

Anderson, R. M., Heesterbeek, H., Klinkenberg, D., & Hollingsworth, T. (2020). How will country-based mitigation measures influence the course of the COVID-19 epidemic? *Lancet, 395*(10228), 931–934.

Bellu, G., Saccomani, M. P., Audoly, S., & D'Angiò, L. (2007). Daisy: A new software tool to test global identifiability of biological and physiological systems. *Computer Methods and Programs in Biomedicine, 88*(1), 52–61.

G Bellu, MP Saccomani, S Audoly, and L D'Angio. Daisy-differential algebra for identifiability of systems.http://daisy.dei.unipd.it.

Bhavana, V., Thakor, P., Singh, S. B., & Mehra, N. K. (2020). COVID-19: Pathophysiology, treatment options, nanotechnology approaches, and research agenda to combating the SARS-CoV2 pandemic. *Life Sciences, 15*(261), Article 118336.

Boulier, F. (2007). Differential elimination and biological modeling. In *Gr$\ddot{o}$bner in Symbolic Analysis*. De Gruyter.

Buchberger, B. (1998). An algorithmical criterion for the solvability of algebraic system of equation. In *Gr$\ddot{o}$bner Bases and Applications*. Cambridge University Press.

Cloutier, M., Nandi, M., Ihsan, A. U., et al. (2020). ADE and hyperinflammation in SARS-CoV2 infection comparison with dengue hemorrhagic fever and feline infectious peritonitis. *Cytokine, 136*, Article 155256.

Eastman, R. T., Roth, J. S., Brimacombe, K. R., et al. (2020). Remdesivir: A review of its discovery and development leading to emergency use authorization for treatment of COVID-19. *ASC Cent Sci, 6*(5), 672–683.

Elbaz, I. M., El-Metwally, H., & Sohaly, M. A. (2023). Viral kinetics, stability and sensitivity analysis of the within-host COVID-19 model. *Scientific Reports, 13*(1), Article 11675.

Esbin, M. N., Whitney, O. N., Chong, S., et al. (2020). Overcoming the bottleneck to widespread testing: A rapid review of nucleic acid testing approaches for COVID-19 detection. *RNA, 26*(7), 771–783.

Gordon, C. J., Tchesnokov, E. P., Feng, J. Y., Porter, D. P., & Gotte, M. (2020). The antiviral compound remdesivir potently inhibits RNA-dependent RNA polymerase from Middle East respiratory syndrome coronavirus. *Journal of Biological Chemistry, 295*(15), 4773–4779.

Guidelines for the use of non-pharmaceutical measures to delay and mitigate the impact of 2019-nCoV. (2020). European Centre for Disease Prevention and Control.

Kampf, G. (2018). Efficacy of ethanol against viruses in hand disinfection. *Journal of Hospital Infection, 98*(4), 331–338.

Li, Q., Guan, X. H., Wu, P., Wang, X. Y., Zhou, L., Tong, Y. Q., et al. (2020a). Early transmission dynamics in Wuhan, China, of novel coronavirus-infected pneumonia. *New England Journal of Medicine, 382*(13), 1199–1207.

Li, C. T., Xu, J. H., Liu, J., Liu, J. W., & Zhou, Y. C. (2020b). The within-host viral kinetics of SARS-CoV-2. *Mathematical Biosciences and Engineering, 17*(4), 2853–2861.

Liu, X., & Wang, X. J. (2020). Potential inhibitors against 2019-nCoV coronavirus M protease from clinically approved medicines. *J Genet Genomics, 47*(2), 119–121.
Marechal, M. L., Morand, P., Epaulard, O., & Nemoz, B. (2020). COVID-19 in clinical practice: A narrative synthesis. *Medecine et Maladies Infectieuses, 50*(8), 639–647.
Miao, H. Y., Xia, X. H., Perelson, A. S., & Wu, H. L. (2011). On identifiability of nonlinear ODE models and applications in viral dynamics. *SIAM Review, 53*(1), 3–39.
Mizumoto, K., Kagaya, K., Zarebski, A., & Chowell, G. (2020). Estimating the asymptomatic proportion of coronavirus disease 2019 (COVID-19) cases on board the diamond princess cruise ship, Yokohama, Japan, 2020. *Euro Surveillance, 25*(10), Article 2000180.
Moghadas, S. M., Shoukat, A., Fitzpatrick, M. C., et al. (2020). Projecting hospital utilization during the COVID-19 outbreaks in the United States. *Proceedings of the National Academy of Sciences of the U S A, 117*(16), 9122–9126.
Nath, B. J., Dehingia, K., Mishra, V. N., Chu, Y. M., & Sarmah, H. K. (2021). Mathematical analysis of a within-host model of SARS-CoV-2. *Advances in Differential Equations, 113*.
Odagaki, T. (2023). New compartment model for COVID-19. *Scientific Reports, 13*(1), 5409.
Okuya, K., Hattori, T., Saito, T., et al. (2022). Multiple routes of antibody-dependent enhancement of SARS-CoV-2 infection. *Microbiology Spectrum, 10*(2), Article e0155321.
Outbreak of acute respiratory syndrome associated with a novel coronavirus, China: First local transmission in the EU/EEA-third update. (2020). European Centre for Disease Prevention and Control.
Pierro, F. D., Iqtadar, S., Khan, A., Ullah, M., et al. (2021). Potential clinical benefits of quercetin in the early stage of COVID-19: Results of a second, pilot, randomized, controlled and open-label clinical trial. *International Journal of General Medicine, 14*, 2807–2816.
Sánchez-Zuno, G. A., Matuz-Flores, M. G., González-Estevez, G., et al. (2021). A review: Antibody-dependent enhancement in COVID-19: The not so friendly side of antibodies. *International Journal of Immunopathology & Pharmacology, 35*, 1–15.
Sanders, J. M., Monogue, M. L., Jodlowski, T. Z., & Cutrell, J. B. (2020). Pharmacologic treatments for coronavirus disease 2019 (COVID-19) a review. *JAMA, 323*(18), 1824–1836.
Shan, S., Wang, R., Zhang, Q., & Zhang, L. (2022). China's first approved novel neutralizing antibody combination therapy against SARS-Cov-2-BRII-196/BRII-198. *Chin J Med Guide, 24*(1), 2–8.
Sims, S., Harris, R., Hussein, S., et al. (2022). Social distancing and isolation strategies to prevent and control the transmission of COVID-19 and other infectious diseases in care homes for older people: An international review. *International Journal of Environmental Research and Public Health, 19*(6), 3450.
Tang, B., Wang, X., Li, Q., Bragazzi, N. L., Tang, S. Y., Xiao, Y. N., & Wu, J. H. (2020). Estimation of the transmission risk of the 2019-nCoV and its implication for public health interventions. *Journal of Clinical Medicine, 9*(2), 462.
Taylor, P. C., Adams, A. C., Hufford, M. M., et al. (2021). Neutralizing monoclonal antibodies for treatment of COVID-19. *Nature Reviews Immunology, 21*(6), 382–393.
Teslya, A., Pham, T. M., Godijk, N. G., Kretzschmar, M. E., Bootsma, M. C. J., & Rozhnova, G. (2020). Impact of self-imposed prevention measures and short-term government-imposed social distancing on mitigating and delaying a COVID-19 epidemic: A modeling study. *PLoS Medicine, 17*(7), Article e1003166.
Tuncer, N., Marctheva, M., LaBarre, B., & Payoute, S. (2018). Structural and practical identifiability analysis of Zika epidemiological models. *Bulletin of Mathematical Biology, 80*(8), 2209–2241.
Tuncer, N., Timsina, A., Nuno, M., Chowell, G., & Martcheva, M. (2022). Parameter identifiability analysis and optimal control of an SARS-CoV-2 model early in the pandemic. *Journal of Biological Dynamics, 16*(1), 412–438.
Wilder-Smith, A., & Freedman, D. O. (2020). Isolation, quarantine, social distancing and community containment: Pivotal role for old-style public health measures in the novel coronavirus (2019-nCoV) outbreak. *Journal of Travel Medicine, 27*(2), Article taaa020.
World Health Organization.https://data.who.int/zh/. Accessed 2023.
Wu, J. T., Leung, K., & Leung, G. M. (2020). Nowcasting and forecasting the potential domestic and international spread of the 2019-nCoV outbreak originating in wuhan, China: A modelling study. *Lancet, 395*(10225), 689–697.
Yu, B., & Chang, J. B. (2022). The first Chinese oral anti-COVID-19 drug Azvudine launched. *Innovation (Camb), 3*(6), Article 100321.
Zheng, S. F., Fan, J., Yu, F., et al. (2020). Viral load dynamics and disease severity in patients infected with SARS-CoV-2 in zhejiang province, China, january-march 2020: Retrospective cohort study. *BMJ, 369*, m1443.